High-performance Piezoelectric Nanogenerators Based on $Cs_2Ag_{0.3}Na_{0.7}InCl_6$ Double Perovskites with High Polarity Induced by Zr/Te Codoping

*Xiangcong He[ab], Jinju Zheng[*b], Tao Yang[c], Deliu Ou[b], Chris R. Bowen[d], Songhan Shi[a], Qiaochu Chen[b], Hui Fu[b], Shuangwu Huang[ae], Yumin Ye[a], Xiaocheng Huang[a], Wenna Liu[*a], Weiyou Yang[*b]*

[a]*Department of Materials Science and Engineering, Faculty of Materials Science and Chemical Engineering, Ningbo University, Ningbo 315211, China*

[b]*Institute of Micro/Nano Materials and Devices, Ningbo University of Technology, Ningbo, 315211, China*

[c]*Beijing Advanced Innovation Center for Materials Genome Engineering, Collaborative Innovation Center of Steel Technology, University of Science and Technology Beijing, Beijing 100083, P. R. China*

[d]*Department of Mechanical Engineering, University of Bath, BA2 7AK, UK.*

[e]*College of Electronic & Information Engineering& Institute of Microelectronics and National Key Laboratory of Shenzhen University, Shenzhen University, Shenzhen 518060, China*

[*] Corresponding authors. E-mail: zhengzhao2007@163.com, liuwenna@nbu.edu.cn, and weiyouyang@tsinghua.org.cn

Graphical Abstract

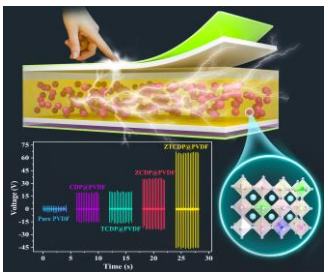

High-performance piezoelectric nanogenerators (PENGs) based on Zr/Te codoped $Cs_2Ag_{0.3}Na_{0.7}InCl_6$ double perovskites (ZTCDPs) are reported. The devices delivered an excellent piezoelectric output, with a maximum open-circuit voltage and short-circuit current density of 67 V and 18 $\mu A \cdot cm^{-2}$, respectively. Moreover, they exhibited significant potential toward the applications of wearable energy harvesters, motion sensors, and self-powered DC devices.

Abstract

Piezoelectric nanogenerators (PENGs), which operate based on mechanical-to-electrical energy conversion, have been widely explored for exciting applications in modern devices such as wearable electronics, self-powered sensors, and energy harvesters. Herein, we report on high-performance PENGs based on $Cs_2Ag_{0.3}Na_{0.7}InCl_6$ double perovskite (CDP) within a polyvinylidene fluoride (PVDF) matrix, which exhibit enhanced polarity due to rationally designed Zr/Te codoping. As a proof of concept, the resultant PENGs based on Zr/Te codoped CDP@PVDF deliver an excellent piezoelectric output, with a maximum open-circuit voltage and short-circuit current density of 67 V and 18 $\mu A \cdot cm^{-2}$. This level of performance is ~19 and ~12 times higher than PVDF-based PENGs with no CDP, and ~2 and ~4 times higher than CDP@PVDF-based PENGs without doping or with single Te doping, and ~1 and ~2 times higher than CDP@PVDF-based PENGs with single Zr doping, respectively. Moreover, the as-assembled PENGs exhibit impressive potential in wearable energy harvesters, motion sensors, and DC-power devices with robust stability, underscoring their bright future toward practical applications.

***Keywords*:** Double perovskites, Doping, Piezoelectric nanogenerator, Polarity

1. Introduction

With the global energy crisis and growth in connected devices for the Internet of Things (IoT), the development and utilization of new sustainable energy and self-powered systems have become a critical challenge [1]. Mechanical energy has inspired significant attention as an alternative form of energy due to the potential rich variety of sources, its non-polluting nature, and ease of availability [2,3]. Piezoelectric nanogenerators (PENGs), which operate based on mechanical-to-electrical energy conversion [4], have been widely explored and applied in wearable electronics [5], self-powered sensors [6], and energy harvesters [7-10]. High-performance PENGs can be fabricated using various piezoelectric materials, including semiconductor materials, ceramic materials, and polymers [11]. However, most semiconductor materials like ZnO have strict environmental requirements due to their chemical instability towards acids and bases. Similarly, piezoelectric ceramics like $BaTiO_3$ are not fully compatible with the fabrication of flexible devices due to their inherent brittleness [7]. Among these materials, piezoelectric polymers have emerged as promising candidates for flexible PENGs on account of their attractive features of high flexibility, good compatibility, ease of processing, and potential for wearable devices operating at modest temperatures [11-13].

As a representative piezoelectric polymer, polyvinylidene fluoride (PVDF), has attracted significant attention for potential application in a PENG [13,14]. It is well known that PVDF is a semi-crystalline polymer, which is primarily composed of five crystalline phases, namely α, β, γ, δ and ε. Among them, the β-phase primarily contributes to its high ferroelectric and piezoelectric properties [6,11,15]. The addition of fillers to the PVDF matrix is a popular method to increase the β-phase content of PVDF induced by the spontaneous polarization of the fillers, and thus enhance the performance of PENGs [16-20]. Moreover, compared with the commonly used approach of polarization by an electric field, the addition of fillers to the PVDF matrix can eliminates the depolarization process that occurs upon removing the electric field,

ensuring the stability of device operation [21]. For instance, a PENG based on $CsPbBr_3$@PVDF demonstrated a voltage output approximately three times higher than that of pure PVDF. This enhancement can be attributed to the elevated β-phase content of PVDF induced by the high polarity $CsPbBr_3$ fillers [22]. Previous studies have reported that the polarity of semiconductor materials can be adjusted through metal ion doping [23,24], offering an attractive approach for enhancing PENG performance. Lead-free double perovskites (DPs, $A_2B_IB_{III}X_6$) can regulate its polarity in a wide range by adjusting their crystal structure and/or doping, making them an attractive candidate for constructing high performance PENGs, which has not been explored until now.

Herein, we devote this work to regulating the polarity of double perovskites to enhance the piezoelectric behavior of PVDF-based PENGs. Firstly, pure CDP, Te doped $Cs_2Ag_{0.3}Na_{0.7}InCl_6$ DP (TCDP), Zr doped $Cs_2Ag_{0.3}Na_{0.7}InCl_6$ DP (ZCDP), and Zr/Te codoped $Cs_2Ag_{0.3}Na_{0.7}InCl_6$ DP (ZTCDP) were synthesized through a hydrothermal method and incorporated into a PVDF matrix. A solution blade coating method was then used to obtain a range of perovskite@PVDF composite films. The incorporation of CDP in a PVDF matrix increased the β-phase content and enhanced their piezoelectric performance, which can be further improved through doping metal ions into the CDP. In addition, the key mechanisms for the enhancement of PVDF piezoelectric performance induced by the increased polarity of double perovskites have been systematically investigated. From the perspective of applicability, the as-prepared PENG was demonstrated to be able to collect various forms of mechanical energy, such as tapping, slapping, twisting, and foot pedaling.

2. Experimental section

2.1. Materials

Zirconium chloride ($ZrCl_4$), tellurium dioxide (TeO_2), cesium chloride (CsCl), silver chloride (AgCl), indium chloride ($InCl_3$), sodium chloride (NaCl), concentrated hydrochloric acid (HCl), N, N-dimethylformamide (DMF) were purchased from

Aladdin. Polyvinylidene fluoride (PVDF, average molecular weight ≈780,000) was purchased from Wuxi United Hengzhou Chemical Co., Ltd. Conductive silver glue was purchased from SINWE, polydimethylsiloxane (PDMS) was purchased from Dow Corning, polyethylene terephthalate (PET) was purchased from Dongsheng plastic materials, aluminum foil was purchased from Ningbo Hangjing Biotechnology Co., Ltd., and polyimide (PI) tape was purchased from Suzhou Yingde Electronics Co., Ltd. Unless otherwise stated, all raw materials were purchased from commercial suppliers and used as raw materials.

2.2. Synthesis of B-site doped $Cs_2Ag_{0.3}Na_{0.7}InCl_6$

The B-site doped $Cs_2Ag_{0.3}Na_{0.7}InCl_6$ double perovskites were synthesized via the hydrothermal method in a muffle oven. If we consider Zr/Te codoped $Cs_2Ag_{0.3}Na_{0.7}InCl_6$ double perovskite as an example: 0.6 mmol $ZrCl_4$, 0.05 mmol TeO_2, 4 mmol CsCl, 0.6 mmol AgCl, 1.4 mmol NaCl, 2 mmol $InCl_3$, and 20 mL HCl were uniformly mixed in a 50 mL Teflon-lined stainless-steel autoclave, followed by transfer into a muffle oven and maintained at 180 °C for 10 h. The resulted products (denoted as ZTCDP) were precipitated with deionized water and then dried at 60 °C for 3 h. CDP and ZCDP were synthesized in the same way, except for no dopant or only a dopant of $ZrCl_4$ was applied, respectively. On considering the feed mole ratio of CsCl, AgCl, NaCl, and $InCl_3$, the as-prepared CDP can thus be named as $Cs_2Ag_{0.3}Na_{0.7}InCl_6$.

2.3. Preparation of B-site doped $Cs_2Ag_{0.3}Na_{0.7}InCl_6$@PVDF composite films

The B-site doped $Cs_2Ag_{0.3}Na_{0.7}InCl_6$@PVDF composite films were prepared by a blade coating method. If we consider the ZTCDP@PVDF composite film as an example. 1.5 g PVDF and 10 mL DMF were loaded into a beaker and completely dissolved into a uniform solution after magnetically stirring at 60 °C for 2 h. Then a certain amount of ZTCDP was added and stirred at 50 °C for 2 h to obtain a uniformly mixed solution. Subsequently, a certain amount of the obtained solution was collected by a pipette gun and placed on a glass plate, spread evenly by a blade coater, and then the glass plate was dried immediately in a vacuum drying oven at 80 °C for 2 h. After natural cooling

to room temperature, the ZTCDP@PVDF composite film with a size of ~1 × 1 cm^2 and thickness of approximately 100 μm was obtained by peeling it off from the glass plate. The CDP@PVDF composite film and the ZCDP@PVDF composite film were prepared in the same way. Moreover, for preparing the ZTCDP@PVDF composite films with different ZTCDP weight ratios, 45 mg, 90 mg, 135 mg, and 180 mg ZTCDP were added into PVDF solution, corresponding to the weight ratios of 3 wt.%, 6 wt.%, 9 wt.% and 12 wt.%, respectively.

2.4. Fabrication of B-site doped $Cs_2Ag_{0.3}Na_{0.7}InCl_6$@PVDF-based PENG

The fabrication method to create a B-site doped CDP@PVDF-based PENG is shown in Fig. 1. If we take the fabrication of a ZTCDP@PVDF-based PENG as an example, the ZTCDP filler, synthesized using the hydrothermal method, was initially introduced into a PVDF/dimethylformamide (DMF) solution, followed by stirring at 50 °C for 2 h. The ZTCDP@PVDF composite film was then prepared using a blade coater. A typical scanning electron microscopy (SEM) image of the resulting films is shown in Fig. S1, indicating a uniform dispersion of the ZTCDP filler in the PVDF matrix. Subsequently, aluminum foil, which was used as the back electrode, was covered into one side of the ZTCDP@PVDF composite film, and the back electrode layer was fixed on the polyethylene terephthalate (PET) sheet and used as a support. Then a layer of PDMS was scraped onto the other side of the composite film and aluminum foil was used as the front electrode to cover the PDMS before it cured. Finally, the electrical connections (leads) were fixed with conductive silver glue and were drawn from the two ends of the back and front electrodes and used for electrical signal testing. Subsequently, the device was packaged with polyimide (PI) tape to obtain the ZTCDP@PVDF-based PENG with the size of ~1 × 1 cm^2. The CDP@PVDF-based PENG and the ZCDP@PVDF-based PENG were fabricated in the same way. The corresponding video on constructing the PENG is presented as the file of SV1 in Supporting Information.

2.5. Characterization

Field emission scanning electron microscopy (FESEM, S-4800, Hitachi, Japan),

transmission electron microscopy (TEM), and high-resolution TEM (HRTEM, JEM-2010, JEOL, Japan) were used to characterize the morphology and structural characteristics of the sample. X-ray diffraction (XRD, D8 Advance, Bruker, Germany) with Cu Kα radiation (λ = 1.5406 Å) and Fourier transform infrared spectroscopy (FTIR, Nicolet 6700, Thermo Fisher Scientific, America) were used to measure the XRD patterns and analyze the phase composition of the composite films. The characteristic polarization-electric field (P-E) loops were measured using a ferroelectric test system (Poly K, America). The d_{33} was recorded by a quasi-static meter (ZJ-3AN, institute of Acoustics, Chinese Academy of Science, China). Differential Scanning Calorimetry (DSC, 214, Netzsch, Germany) was used to measure the melting enthalpy and crystallinity of the samples. X-ray photoelectron spectroscopy (XPS, ESCALAB 250Xi, Thermo Fisher Scientific, USA) and 700 Series inductively coupled plasma optical emission spectrometer (ICP-OES, Agilent Technologies, California, USA) analysis were conducted to get the concentration of B-site cations such as Ag^{+}, Na^{+}, In^{3+}, Zr^{4+}, and Te^{4+} in metal-doped $Cs_2Ag_{0.3}Na_{0.7}InCl_6$. A blade coater (MSK-AFA-IIID, Hefei Kejing Materials Technology Co., Ltd., China) was used to prepare the composite films. An LCR meter (TH 2838A, Changzhou Tonghui Electronics Co., Ltd., China) was used to record the dielectric constant within the frequency range from 1 to 10^3 kHz. Linear motor (Shengda Machinery, China), digital storage oscilloscope (SDS5032X, Siglent, Germany), and programmable electrometer (Keithley Model 6517A, America) were used to test the electrical output signals of PENGs under different external forces and operating frequencies. When testing, a linear motor was used to output repeated pressure, and a digital storage oscilloscope and a programmable electrometer were used to collect the electrical output signals of the as-prepared PENGs. The intrinsic electrical output signals of load matching and energy storage were collected by connecting a full-wave bridge rectifier circuit to convert the AC signals into a DC signal.

3. Results and discussion

3.1. Characterization of pristine and B-site doped $Cs_2Ag_{0.3}Na_{0.7}InCl_6$@PVDF composite films

Fig. 2 shows the XPS spectra of the as-prepared CDP, ZCDP, and ZTCDP fillers. Related data on the TCDP filler are not provided due to inconspicuous improvement in the piezoelectric performance of as-constructed devices resulting from the very low concentration of Te dopant. The survey spectra in Fig. 2a reveal the existence of all elements added, indicating the successful doping of CDP with Zr and Te elements. High-resolution scans of Ag 3*d*, In 3*d*, Na 1*s*, Zr 3*d*, and Te 3*d* are provided in Fig. 2b-f. The Ag 3*d* peaks (Fig. 2b) which are centered at 368.2 eV and 374.1 eV are assigned to Ag $3d_{5/2}$ and Ag $3d_{3/2}$ and suggest that the Ag element is in the form of Ag^+. It is worth noting that, compared to CDP, these two peaks shift to a lower binding energy by 0.3 eV in ZCDP and 0.1 in ZTCDP. This phenomenon confirms the presence of electronic coupling between CDP and the Zr/Te doping elements [25]. The In 3*d* peaks (Fig. 2c) with binding energies at 445.5 and 452.9 eV correspond to In $3d_{5/2}$ and In $3d_{3/2}$, respectively, suggesting that the chemical state of In is In^{3+}. In addition, a similar shift of the In 3*d* peaks derives from the electron density transformation of the In atoms after doping with Zr and Te [26]. Fig. 2d shows the Na 1*s* peak is centered at 1071.5 eV, suggesting the chemical state of Na is Na^+. However, the peak shifts are in the opposite direction after Zr/Te doping, compared with those of Ag and In, which is attributed to the inverse regular of electron density transformation of Na atoms. The Zr 3*d* high-resolution peaks (Fig. 2e) are assigned to Zr $3d_{5/2}$ (182.5 eV) and Zr $3d_{3/2}$ (184.9 eV) respectively. This indicates the existence of the chemical state Zr^{4+} in the ZCDP and ZTCDP. The high-resolution Te 3*d* spectrum (Fig. 2f) exhibits two peaks at 572.9 eV (Te $3d_{5/2}$) and 580.1 eV (Te $3d_{3/2}$), confirming the existence of Te^{4+} in ZTCDP [27]. In addition, the ICP results in Table S1 further indicated that Zr^{4+} and/or Te^{4+} was successfully doped into the host of CDP and partially replaced the B-site elementals of In^{3+} [28].

The morphology and detailed structural characteristics of the composite films are

187 analyzed by TEM and FESEM. Typical TEM (Fig. 3a) and SEM (Fig. S1) images of
188 the ZTCDP@PVDF composite film verify that ZTCDPs are successfully dispersed in
189 PVDF matrix. The corresponding HRTEM image (Fig. 3b) clearly shows the (422)
190 crystal plane of cubic ZTCDP and the β-phase (100) plane of PVDF, confirming the
191 uniform mixing of the perovskite and PVDF. The TEM, HRTEM, and corresponding
192 selected area electron diffraction (SAED) patterns of pure PVDF, CDP@PVDF, and
193 ZCDP@PVDF are also shown in Fig. S2. In addition, the successful doping of Zr^{4+} in
194 CDP was further confirmed by the contracted interplanar spacing of the (444) plane of
195 ZCDP.
196 The crystallinity of the pure PVDF, CDP@PVDF, ZCDP@PVDF, and
197 ZTCDP@PVDF composite films was measured using differential scanning calorimetry
198 (DSC) (Fig. S3). The degree of mass crystallinity ($x_c(\%)$) was calculated based on the
199 melting enthalpy of the heating trace (ΔH_m) using the following formula
200 $x_c(\%)=\Delta H_m/\Delta H_0 \times 100\%$ (where ΔH_0 =104.6 J/g represents the fusion heat of 100%
201 crystalline PVDF, and ΔH_m is the melting enthalpy) [29]. The corresponding melting
202 enthalpy was determined by fitting the peak area of the DSC thermograms, and the
203 calculated ΔH_m and $x_c(\%)$ values are presented in Table S2. The crystallinity increased
204 slightly from 51.06% of pure PVDF to 53.28% of ZTCDP@PVDF, indicating the
205 crystallinity has no significant influence on the piezoelectric properties of the composite
206 films.
207 To investigate the effect of double perovskite fillers on the β-phase content in PVDF,
208 the crystallographic structure of pure PVDF and the perovskite@PVDF composite
209 films were determined using XRD. As shown in Fig. 3c, for the pure PVDF film the
210 diffraction peaks of α-phase (020), (111), (041), and β-phase (110) match those in the
211 reported work [30]. In the composite films, diffraction peaks were detected at 14.4°,
212 23.8°, 29.3°, 34.1°, 42.0°, 48.8°, 55.2°, and 60.9°, which correspond to the (111), (220),
213 (222), (400), (422), (440), (620), and (444) planes of CDP material, respectively [31].
214 More importantly, with the incorporation of CDP, ZCDP, and ZTCDP in PVDF, the

diffraction peaks of α-phase (020) and (111) of PVDF gradually disappear, while a much larger diffraction peak of the β-phase (110) plane is detected. The proportions of the phase content ($C_{\beta/\alpha}$) of pure PVDF and composite films were calculated based on the β-phase and α-phase planes. As shown in Table S3, the $C_{\beta/\alpha}$ increases gradually with the incorporation of CDP, ZCDP, and ZTCDP into PVDF, and reaches a maximum of $C_{\beta/\alpha}$ = 2.35 in the ZTCDP@PVDF composite film.

FTIR also confirms the positivity of the high polarity double perovskite in inducing the transition of PVDF from α-phase to β-phase. As shown in Fig. 3d, the peaks of the α-phase decrease, or even disappear on incorporating CDP, ZCDP, and ZTCDP in PVDF, while that of the β-phase rise significantly. The proportion of electroactive content of the β-phase (F_β) can be calculated by Equation 1 [11].

$$F_{(\beta)} = \frac{A_\beta}{\left(\frac{K_\beta}{K_\alpha}\right)A_\alpha + A_\beta} \times 100\ \% \quad (1)$$

Where A_β and A_α are the absorbances at 840 cm^{-1} and 766 cm^{-1}. K_β and K_α represent the corresponding absorption coefficients of 7.7×10^4 and 6.1×10^4 cm^2 mol^{-1}, respectively. As shown in Table S4, the F_β gradually increases with the incorporation of CDP, ZCDP, and ZTCDP in PVDF, and reaches a maximum of 84.5% in the ZTCDP@PVDF composite film, which is higher than that of pure PVDF of 39.0%. These results demonstrate that the incorporation of CDP induces the transition of the α-phase to the β-phase of PVDF, and the doping of Zr^{4+} and Te^{4+} metal ions in CDP promotes this transition.

As is known, the β-phase content of PVDF film is significantly influenced by the spontaneous/electric field polarization of the composite films, and it is closely associated with the dielectric constant (ε) [32]. Fig. 4a shows the dielectric constants of CDP, ZCDP, and ZTCDP, and their PVDF composite films. On doping with Zr^{4+} and/or Te^{4+}, the dielectric constant increased from 7.51 (CDP) to 19.46 (ZCDP) and 22.41 (ZTCDP) at 100 kHz, respectively, indicating an enhancement in the polarity of ZCDP and ZTCDP, due to the positive correlation between them [32]. The high polarity of ZTCDP can be attributed to the partly heterovalent replacement of B-site cations in

CDP by the tetravalent ions such as Zr^{4+} and Te^{4+}, which enable an increased quantity of charge in their charge center and/or a stronger deviation of their electron cloud, and thus an enhancement in the molecular polarity of CDP by Zr^{4+} and Te^{4+} doping [24]. As expected, the dielectric constants of pure PVDF, CDP@PVDF, ZCDP@PVDF, and ZTCDP@PVDF composite films also gradually increase (Fig. 4b), which are 9.46, 14.61, 18.34, and 20.08 at 100 kHz, respectively. Remarkably, the dielectric constant of the ZTCDP@PVDF composite film is more than one times higher than that of pure PVDF, indicating an effective polarization caused by Zr^{4+}/Te^{4+} doping in CDP filler.

To analyze the ferroelectric properties and the spontaneous polarization of the composite films, the polarization-electric field (*P*-*E*) hysteresis loops of CDP, ZCDP, and ZTCDP were measured with an applied electric field of 0.25 MV/m. As shown in Fig. 4c, all samples possess some ferroelectricity and the doping of Zr^{4+}/Te^{4+} can enhance the ferroelectric properties of CDP. As is well-known, the intersection of the *P*-*E* hysteresis loops with the vertical axis indicates the remnant polarization (P_r), the intersection with the horizontal axis represents the coercive field (E_c), and the intersection of the tangent of the highest value of the *P*-*E* hysteresis loops with the vertical axis represents the spontaneous polarization (P_s). Generally, a larger maximum value of the *P*-*E* hysteresis loops corresponds to a great level of spontaneous polarization [9]. As expected, the *P*-*E* hysteresis loops of the ZTCDP@PVDF composite film (Fig. 4d) exhibit the maximum P_r, P_s, and E_c, indicating improved ferroelectric properties and spontaneous polarization. In addition, to directly assess their piezoelectric properties, the piezoelectric coefficient (d_{33}) of the pure PVDF, CDP@PVDF, ZCDP@PVDF, and ZTCDP@PVDF films are measured by a quasi-static meter, and the results are provided in the inset of Fig. 4d and Table S5. It suggests that the d_{33} value of the ZTCDP@PVDF composite film is ~4 times higher than that of pure PVDF (from 4.5 pC N^{-1} to 23.4 pC N^{-1}). The above results confirm the high level of ferroelectricity and spontaneous polarization in the ZTCDP@PVDF composite film.

The enhanced piezoelectric properties of PVDF films filled with doped CDP can be

attributed to the following mechanism. Firstly, the incorporation of perovskite fillers creates multiple interfacial regions within the PVDF matrix, owing to the significant difference in dielectric properties between the perovskite phase and PVDF. Consequently, charged layers are formed in the vicinity of the perovskite nanoparticles, stemming from immobile charged impurities, trapped carriers, and mobile electrons and hole [33]. These charged layers give rise to a built-in electric field [22], leading to the spontaneous polarization of the charged layers and the subsequent transition of PVDF from the α-phase to β-phase [22,34-37]. This transition enhances the piezoelectric performance of the PVDF film, thereby improving its overall piezoelectric properties upon incorporation of CDP perovskite fillers.

Secondly, we investigate why a doped CDP with Zr^{4+}/Te^{4+} can further improve the piezoelectric properties of the composite films. As is known, the polarity of a molecule is determined by its dipole moment, which is the product of the distance between the positive and negative charge centers and the charge magnitude. In this study, Zr^{4+}/Te^{4+} doping in CDP perovskite (e.g., ZTCDP) involves the partial heterovalent substitution of B-site cations with tetravalent ions, such as Zr^{4+} and Te^{4+}. This substitution increases the charge quantity in the charge centers and/or induces a stronger deviation of the electron cloud, resulting in an increased dipole moment and molecular polarity. Consequently, these perovskites exhibit enhanced dipole polarization under the influence of built-in electric field generated by the interface effect, leading to the accumulation of more aggregate charges and a higher dielectric constant [33,38-42]. Namely, incorporating double perovskites with higher polarity into the PVDF matrix results in a more pronounced polarity difference, leading to a stronger degree of charge accumulation at the interface between the two regions. This accumulation enables a stronger built-in electric field within the PVDF matrix, thereby inducing an enhanced spontaneous polarization effect. Consequently, the accelerated transition of PVDF from the α-phase to β-phase is achieved, resulting in higher piezoelectric performance of the composite films.

3.2. Electrical output performance of ZTCDP@PVDF-based PENG

To further evaluate the potential of ZTCDP@PVDF composite film for device applications, a PENG was constructed based on a ZTCDP@PVDF composite. As a control, PENGs based on pure PVDF, CDP@PVDF, TCDP@PVDF, and ZCDP@PVDF were also assembled. The open-circuit voltage (V_{oc}) and the short-circuit current density (I_{sc}) of PENGs based on pure PVDF and composite films were evaluated at 50 N and 3 Hz are shown in Fig. 5a, b, respectively. With the introduction of DP fillers into PVDF, both V_{oc} and I_{sc} show a significant increase. The V_{oc} rise from 3.1 V of a PVDF-based PENG to 67 V (also see the video of SV2 in Supporting Information) of a ZTCDP@PVDF-based PENG, while the I_{sc} increase from 1.4 μA·cm^{-2} to 18 μA·cm^{-2}, respectively (also see the video of SV3 in Supporting Information). An approximately 20-fold and 13-fold increase in V_{oc} and I_{sc}, respectively, was therefore obtained by creating the ZTCDP@PVDF composite. Meanwhile, compared with CDP@PVDF-based PENG (V_{oc}: ~ 18.8 V, I_{sc}: ~ 3.9 μA·cm^{-2}) and TCDP@PVDF-based PENG (V_{oc}: ~ 19.1 V, I_{sc}: ~ 4.2 μA·cm^{-2}), the piezoelectric performance of ZTCDP@PVDF-based PENG show approximately 3-fold and 5-fold increase in V_{oc} and I_{sc}, respectively. Similarly, there is approximately 2-fold and 3-fold increase in V_{oc} and I_{sc}, respectively, as compared with those of ZCDP@PVDF-based PENG (V_{oc}: ~ 35.2 V, I_{sc}: ~ 6.4 μA·cm^{-2}).

In terms of the fact that PVDF has high triboelectric charge densities, the PENGs fabricated with PVDF are likely to exhibit triboelectric contributions in their electrical output signals. The most common source of contact electrification in PENGs comes from the friction between the loading object and encapsulating polymer (*i.e.,* in our case, PI). Additionally, the interfacial slip among the piezoelectric polymer and encapsulating polymer and/or the metallic electrodes during testing also induces contact electrification [43]. To disclose the triboelectric contributions in the former case, a series of comparison experiments are performed on PENGs with and without PDMS (as adhesive) and PI materials for showing their triboelectric contribution in the resultant

signals. As shown in Fig. S4, the electrical output signals under both conditions are found to be nearly identical, suggesting that the triboelectric contributions resulting from the friction between PI and the test equipment could be ignored. Regardless of the fact that the identification of triboelectric contributions in the latter case has proved challenging based on currently available data, the d_{33} data could be used to directly characterize the piezoelectric properties of DP@PVDF films. As discussed above, the d_{33} value of ZTCDP@PVDF film is ~4 times higher than that of pure PVDF, indicating a significantly enhanced piezoelectric properties of DP@PVDF-based PENGs with the incorporation of Zr/Te into DPs.

The performance of the PENGs based on ZTCDP@PVDF with different ZTCDP contents were also characterized to explore the effect of ZTCDP filler on piezoelectric properties. Fig. 5c, d show the V_{oc} and I_{sc} of PENGs with a ZTCDP content of 0 wt.%, 3 wt.%, 6 wt.%, 9 wt.%, and 12 wt.%, respectively under the test conditions of 50 N and 3 Hz. Noticeably, with an increase of the ZTCDP weight ratio, the piezoelectric signals significantly increase and reach a maximum value of 67 V (V_{oc}) and 18 $\mu A \cdot cm^{-2}$ (I_{sc}) at a ZTCDP weight ratio of 9 wt.%, and then decrease with a further increase of ZTCDP (12 wt.%). The initial increase of the piezoelectric signals is mainly due to the enhanced built-in electric field caused by the increased interfacial regions between the fillers and PVDF with increasing weight ratio of ZTCDP. Which leads to a higher spontaneous polarization and thereby improves a greater level of phase transition of PVDF from the α-phase to β-phase [33], as confirmed by the XRD (Fig. S5) and FTIR (Fig. S6). When the ZTCDP incorporation exceeds 9 wt.%, the piezoelectric signals exhibit a decrease, which is accompanied by a decrease in its d_{33} coefficient (Fig. S7); this could be attributed to the agglomeration of the ZTCDPs in the PVDF matrix as shown in Fig. S8. The formation of agglomerates of ZTCDPs decreases the interfacial regions between the fillers and PVDF, and thus hampers the phase transition of PVDF. These results show that ZTCDP can effectively improve the piezoelectric performances of PVDF and obtain the best performance at a weight ratio of 9 wt.%; this weight ratio

(9 wt.%) was therefore selected for subsequent testing.

To simulate real applications conditions, the piezoelectric performance of a ZTCDP@PVDF-based PENG at different frequencies and force levels were evaluated. As shown in Fig. 6a, b, under a test condition of 50 N, the V_{oc} and I_{sc} gradually increase with the increase of the frequency from 0.5 Hz to 5 Hz, which may be attributed to the enhanced driving force and increased frequencies; for example, I_{sc} is proportional to dF/dt, where F is force. Moreover, under a test condition of 3 Hz, the piezoelectric signals of the PENG gradually increase with increasing force levels (1-50 N), as shown in Fig. 6c, d. This can be attributed to the increased deformation and dipole polarization in the piezoelectric composite films, thereby providing more induced charges that accumulate on the surface of the front and back electrodes, resulting in larger piezoelectric signals [9]. This performance enables the potential application of ZTCDP@PVDF-based PENG on pressure sensors.

Fig. 7 shows the power density of the ZTCDP@PVDF-based PENG for different external load resistances (1-200 MΩ). The V_{oc} gradually rises steadily from 1.40 V to 29.2 V while the I_{sc} decreases gradually from 10 μA·cm^{-2} to 0.87 μA·cm^{-2}. The corresponding power density is calculated by the equation $P=V^2/R$ (where V and R represent the measured V_{oc} and the corresponding external load resistance) [44] and reaches the maximum value of 7.56 μW·cm^{-2} at 20 MΩ; the maximum power output corresponding to the condition with the impedance of the electrical load matches the electrical impedance of the piezoelectric nanogenerator. This result verifies that as an energy harvesting device, the ZTCDP@PVDF-based PENG is sensitive in a large load resistance range.

3.3. Application and stability of ZTCDP@PVDF-based PENG

As a result of its excellent stability over a wide frequency range, and high sensitivity upon external force and resistance, the ZTCDP@PVDF-based PENG was employed as a wearable energy harvesting device for real-time operation. Fig. 8a-d show the V_{oc} signals under different body movements such as fist beating, finger tapping, elbow

bending, and foot treading. The PENG exhibits a diverse range of waveforms and disparate amplitudes of electrical output signals for different motions. The V_{oc} reaches a minimum value (~4V) upon finger tapping and a maximum value (~20V) under foot stepping. This phenomenon can be ascribed to the different mechanical deformation levels and strains of the PENG subjected to the range of body movements. The signals change consistently with the corresponding motions, indicating the high reliability of the PENG in motion detection. Furthermore, considering the potential application, the stability of the PENG was assessed for over 4000 cycles of consecutive strikes under 40 N. As shown in Fig. 8e, the PENG exhibits a steady electrical output during the whole test, indicating excellent stability of the prepared device. To demonstrate the application of the ZTCDP@PVDF-based PENG in DC-power devices, the PENG is used to charge capacitors of different levels of capacitance (Fig. 8f, inset is the rectifier circuit diagram). For different capacitors, after charging for 20 s, the voltages reach up to 0.9 V (1 μF), 0.6 V (2.2 μF), and 0.4 V (3.3 μF), respectively; all capacitors are fully charged within 40 s. In addition, two LED lights were successfully illuminated using the PENG as shown in Fig. 8g, and the corresponding videos are presented in SV4 and SV5 in Supporting Information. Table 1 provides an overview on the key piezoelectric outputs of a range of perovskite and PVDF related PENGs typically reported previously. Notably, our ZTCDP@PVDF-based PENGs display superior performances to most perovskite@PVDF-based analogues, of which the V_{oc} and I_{sc} are ~13 and ~6 times to those of DP@PVDF-based PENGs ever reported [18].

4. Conclusions

In summary, we have demonstrated the manufacture of high-performance PENGs based on $Cs_2Ag_{0.3}Na_{0.7}InCl_6$ double perovskites filled in PVDF, which is primarily attributed to their significantly enhanced polarity by the Zr/Te codoping. It is confirmed that the incorporated CDPs into the PVDF matrix could remarkably increase the β-phase content of PVDF, which is induced by the rationally designed Zr and Te dopants for

enabling the formation of a strong built-in electric field and improved polarity of $Cs_2Ag_{0.3}Na_{0.7}InCl_6$ crystals, thereby enhancing the piezoelectric and ferroelectric properties of the target PENGs. As a result, the as-fabricated ZTCDP@PVDF has a high β-phase electroactive content up to ~84.5%, a high piezoelectric coefficient up to 23.4 pC N^{-1}, and a high level of ferroelectricity. Correspondingly, the as-constructed PENGs exhibit a high open-circuit voltage (V_{oc} ~ 67 V) and short-circuit current density (I_{sc} ~ 18 μA·cm^{-2}), which are ~19 and ~12 times higher than PVDF-based PENGs without CDPs and doping, and ~2 and ~4 times higher than CDP@PVDF-based PENGs without doping or with single Te doping, and ~1 and ~2 times higher than CDP@PVDF-based PENGs with single Zr doping, respectively. Furthermore, the as-assembled PENGs behave significant potential toward the applications in wearable energy harvesters, motion sensors, and DC-power devices with robust stability. This work provides new insights and inspiration for the development of advanced piezoelectric nanogenerators.

CRediT authorship contribution statement

Xiangcong He: Conceptualization, Formal analysis, Methodology, Investigation, Visualization, Data curation, Writing – original draft. **Jinju Zheng**: Methodology, Formal analysis, Conceptualization, Project administration, Supervision, Discussion, Manuscript revision, Funding acquisition, Writing – review & editing. **Tao Yang**: Methodology, Formal analysis, Conceptualization, Discussion. **Deliu Ou**: Methodology, Visualization, Software. **Chris R. Bowen**: Writing – review & editing. **Songhan Shi**: Methodology, Data curation. **Qiaochu Chen**: Investigation. **Hui Fu**: Investigation. **Shuangwu Huang**:Writing – review & editing. **Yumin Ye**: Writing – review & editing. **Xiaocheng Huang**: Manuscript revision. **Wenna Liu**: Conceptualization, Methodology, Discussion, Manuscript revision, Funding acquisition, Writing – review & editing. **Weiyou Yang**: Discussion, Manuscript revision, Project administration, Supervision, Funding acquisition, Writing – review & editing.

Declaration of Competing Interest

The authors declare that they have no known competing financial interests or personal relationships that could have appeared to influence the work reported in this paper.

Acknowledgements

This work was supported by the National Natural Science Foundation of China (62104121), the Natural Science Foundations of Zhejiang Province (LGJ20E020002 and LQ22E020002), and the Ningbo Science & Technology Innovation Research Programs (2020Z061 and 2021Z058).

Appendix A. Supporting information

Supplementary data associated with this article can be found in the online version at.

References

[1] B. Crew, Solving the energy crisis, Nature 609 (2022), S1.

[2] J. Luo, Z.L. Wang, Recent advances in triboelectric nanogenerator based self-charging power systems, Energy Stor. Mater. 23 (2019), 617-628.

[3] X. Wang, J. Song, J. Liu, Z.L. Wang, Direct-current nanogenerator driven by ultrasonic waves, Science 316 (2007), 102-105.

[4] K. Dong, X. Peng, Z.L. Wang, Fiber/fabric-based piezoelectric and triboelectric nanogenerators for flexible/stretchable and wearable electronics and artificial intelligence, Adv. Mater. 32 (2020), 1902549.

[5] F.R. Fan, W. Tang, Z.L. Wang, Flexible nanogenerators for energy harvesting and self-powered electronics, Adv. Mater. 28 (2016), 4283-4305.

[6] X. Cao, Y. Xiong, J. Sun, X. Zhu, Q. Sun, Z. Wang, Piezoelectric nanogenerators derived self-powered sensors for multifunctional applications and artificial intelligence, Adv. Funct. Mater. 31 (2021), 2102983.

[7] L. Zhou, T. Yang, L. Zhu, W. Li, S. Wang, X. Hou, X. Mao, Z. Wang, Piezoelectric nanogenerators with high performance against harsh conditions based on tunable N doped 4H-SiC nanowire arrays, Nano Energy 83 (2021), 105826.

[8] L. Zhou, L. Zhu, T. Yang, X. Hou, Z. Du, S. Cao, H. Wang, K.C. Chou, Z. Wang, Ultra-stable and durable piezoelectric nanogenerator with all-weather service capability based on N doped 4H-SiC nanohole arrays, Nanomicro Lett. 14 (2021), 30.

[9] S. Shi, Z. Pan, Y. Cheng, Y. Zhai, Y. Zhang, X. Ding, J. Liu, J. Zhai, J. Xu, Three-dimensional polypyrrole induced high-performance flexible piezoelectric nanogenerators for mechanical energy harvesting, Compos. Sci. Technol. 219 (2022), 109260.

[10] S. Lee, S.-H. Bae, L. Lin, Y. Yang, C. Park, S.-W. Kim, S. Cha, H. Kim, Y.J. Park, Z. Wang, Super-flexible nanogenerator for energy harvesting from gentle wind and as an active deformation sensor, Adv. Funct. Mater. 23 (2013), 2445-2449.

[11] S.D. Mahapatra, P.C. Mohapatra, A.I. Aria, G. Christie, Y.K. Mishra, S. Hofmann,

V.K. Thakur, Piezoelectric materials for energy harvesting and sensing applications: roadmap for future smart materials, Adv. Sci. 8 (2021), 2100864.

[12] A.J. Lovinger, Ferroelectric polymers, Science 220 (1983), 1115-1121.

[13] J. Nie, L. Zhu, W. Zhai, A. Berbille, L. Li, Z. Wang, Flexible piezoelectric nanogenerators based on P(VDF-TrFE)/$CsPbBr_3$ quantum dot composite films, ACS Appl. Electron. Mater. 3 (2021), 2136-2144.

[14] J. Yi, Y. Song, Z. Cao, C. Li, C. Xiong, Gram-scale Y-doped ZnO and PVDF electrospun film for piezoelectric nanogenerators, Compos. Sci. Technol. 215 (2021), 109011.

[15] P. Martins, A.C. Lopes, S. Lanceros-Mendez, Electroactive phases of poly(vinylidene fluoride): determination, processing and applications, Prog. Polym. Sci. 39 (2014), 683-706.

[16] A. Sultana, P. Sadhukhan, M.M. Alam, S. Das, T.R. Middya, D. Mandal, Organo-lead halide perovskite induced electroactive β-phase in porous PVDF films: an excellent material for photoactive piezoelectric energy harvester and photodetector, ACS Appl. Mater. Interfaces 10 (2018), 4121-4130.

[17] S.H. Wankhade, S. Tiwari, A. Gaur, P. Maiti, PVDF-PZT nanohybrid based nanogenerator for energy harvesting applications, Energy Rep. 6 (2020), 358-364.

[18] Z. Mallick, D. Saini, R. Sarkar, T.K. Kundu, D. Mandal, Piezo-phototronic effect in highly stable lead-free double perovskite Cs_2SnI_6-PVDF nanocomposite: possibility for strain modulated optical sensor, Nano Energy 100 (2022), 107451.

[19] W. Zhai, J. Nie, L. Zhu, Enhanced flexible poly(vinylidene fluoride-trifluorethylene) piezoelectric nanogenerators by SnSe nanosheet doping and solvent treatment, ACS Appl. Mater. Interfaces 13 (2021), 32278-32285.

[20] X. Du, Z. Zhou, Z. Zhang, L. Yao, Q. Zhang, H. Yang, Porous, multi-layered piezoelectric composites based on highly oriented PZT/PVDF electrospinning fibers for high-performance piezoelectric nanogenerators, J. Adv. Ceram. 11 (2022), 331-344.

[21] N.A. Shepelin, A.M. Glushenkov, V.C. Lussini, P.J. Fox, G.W. Dicinoski, J.G.

Shapter, A.V. Ellis, New developments in composites, copolymer technologies and processing techniques for flexible fluoropolymer piezoelectric generators for efficient energy harvesting, Energy Environ. Sci. 12 (2019), 1143-1176.

[22] Y. Xue, T. Yang, Y. Zheng, E. Wang, H. Wang, L. Zhu, Z. Du, X. Hou, K.-C. Chou, The mechanism of PVDF/$CsPbBr_3$ perovskite composite fiber as self-polarization piezoelectric nanogenerator with ultra-high output voltage, J. Mater. Chem. A 10 (2022), 21893-21904.

[23] Z. Liliental-Weber, M. Benamara, W. Swider, J. Washburn, I. Grzegory, S. Porowski, D.J.H. Lambert, C.J. Eiting, R.D. Dupuis, Mg-doped GaN: similar defects in bulk crystals and layers grown on Al_2O_3 by metal–organic chemical-vapor deposition, Appl. Phys. Lett. 75 (1999), 4159-4161.

[24] C. Jin, N. Hao, Z. Xu, I. Trase, Y. Nie, L. Dong, A. Closson, Z. Chen, J.X.J. Zhang, Flexible piezoelectric nanogenerators using metal-doped ZnO-PVDF films, Sens. Actuator A Phys. 305 (2020), 111912.

[25] Y. Wang, C. Yan, C. Li, Z. Lu, C. Ma, Y. Yan, Y. Zhang, Charge transfer tuned by the surrounding dielectrics in TiO_2-Ag composite arrays, Nanomaterials 8 (2018), 8121019.

[26] H. Yang, J. Tang, Y. Luo, X. Zhan, Z. Liang, L. Jiang, H. Hou, W. Yang, MOFs-derived fusiform In_2O_3 mesoporous nanorods anchored with ultrafine CdZnS nanoparticles for boosting visible-light photocatalytic hydrogen evolution, Small 17 (2021), 2102307.

[27] T. Chang, Q. Wei, R. Zeng, S. Cao, J. Zhao, B. Zou, Efficient energy transfer in Te^{4+}-doped Cs_2ZrCl_6 vacancy-ordered perovskites and ultrahigh moisture stability via A-site Rb-alloying strategy, J. Phys. Chem. Lett. 12 (2021), 1829-1837.

[28] Q. Chen, H. Fu, J. Jiang, Z. Fang, H. Zhang, W. Yang, W. Liu, J. Zheng, Zr^{4+} and Bi^{3+} codoped $Cs_2Ag_{0.3}Na_{0.7}InCl_6$ double perovskite for single-composition white-light emitting phosphors and multimodal optical anti-counterfeiting, J. Lumin. 258 (2023), 119783.

[29] S. Mohamadi, N. Sharifi-Sanjani, Crystallization of PVDF in graphene-filled electrospun PVDF/PMMA nanofibers processed at three different conditions, Fibers Polym. 17 (2016), 582-592.

[30] S. Mondal, T. Paul, S. Maiti, B.K. Das, K.K. Chattopadhyay, Human motion interactive mechanical energy harvester based on all inorganic perovskite-PVDF, Nano Energy 74 (2020), 104870.

[31] S. Saikia, A. Joshi, H. Arfin, S. Badola, S. Saha, A. Nag, Sb^{3+}-Er^{3+}-codoped $Cs_2NaInCl_6$ for emitting blue and short-wave infrared radiation, Angew. Chem. Int. Ed. 61 (2022), 202201628.

[32] W. Zheng, Z. Li, K. Chen, S. Liu, Z. Chi, J. Xu, Y. Zhang, Temperature-resistant intrinsic high dielectric constant polyimides: more flexibility of the dipoles, larger permittivity of the materials, Molecules 27 (2022), 6337.

[33] G. Du, J. Wang, Y. Liu, J. Yuan, T. Liu, C. Cai, B. Luo, S. Zhu, Z. Wei, S. Wang, S. Nie, Fabrication of advanced cellulosic triboelectric materials via dielectric modulation, Adv. Sci. 8 (2023), 2206243.

[34] X. Fan, Z. Wu, L. Wang, C. Wang, Exploring the origin of high dechlorination activity in polar materials $M_2B_5O_9Cl$ (M = Ca, Sr, Ba, Pb) with built-in electric field, Chem. Mater. 29 (2016), 639-647.

[35] M. Pusty, L. Sinha, P.M. Shirage, A flexible self-poled piezoelectric nanogenerator based on a rGO−Ag/PVDF nanocomposite, New J. Chem. 43 (2019), 284-294.

[36] S. Bodkhe, G. Turcot, F.P. Gosselin, D. Therriault, One-step solvent evaporation-assisted 3D printing of piezoelectric PVDF nanocomposite structures, ACS Appl. Mater. Interfaces 9 (2017), 20833-20842.

[37] N.A. Shepelin, P.C. Sherrell, E. Goudeli, E.N. Skountzos, V.C. Lussini, G.W. Dicinoski, J.G. Shapter, A.V. Ellis, Printed recyclable and self-poled polymer piezoelectric generators through single-walled carbon nanotube templating, Energy Environ. Sci. 13 (2020), 868-883.

[38] M. Li, J. Sun, G. Chen, S. Yao, B. Cong, Construction double electric field of

564 sulphur vacancies as medium ZnS/Bi_2S_3-PVDF self-supported recoverable
565 piezoelectric film photocatalyst for enhanced photocatalytic performance, Appl. Catal.
566 B 301 (2022), 120792.
567 [39]G. Sun, M. Jin, Q. Liu, C. Zhang, J. Pan, Y. Wang, X. Gao, G. Sun, X. Pan, J. Zhou,
568 Unveiling the enhancement essence on Li_2S deposition by the polarized topological β-
569 polyvinylidene fluoride: beyond built-in electric field effect, Chem. Eng. J. 453 (2023),
570 139752.
571 [40]L. Zhang, J. Sha, G. Sun, R. Chen, Q. Liu, J. Liu, J. Yu, H. Zhang, J. Wang, Vacancy
572 engineering and constructing built-in electric field in Z-scheme full-spectrum-response
573 0D/3D BiOI/$MoSe_2$ heterojunction modified PVDF membrane for PPCPs degradation
574 and anti-biofouling, Chem. Eng. J. 414 (2021), 128867.
575 [41]N. Soin, D. Boyer, K. Prashanthi, S. Sharma, A.A. Narasimulu, J. Luo, T.H. Shah,
576 E. Siores, T. Thundat, Exclusive self-aligned beta-phase PVDF films with abnormal
577 piezoelectric coefficient prepared via phase inversion, Chem. Comm. 51 (2015), 8257-
578 8260.
579 [42]C. Chen, S. Zhao, C. Pan, Y. Zi, F. Wang, C. Yang, Z.L. Wang, A method for
580 quantitatively separating the piezoelectric component from the as-received
581 "piezoelectric" signal, Nat. Commun. 13 (2022), 1391.
582 [43] A. Sutka, P.C. Sherrell, N.A. Shepelin, L. Lapcinskis, K. Malnieks, A.V. Ellis,
583 Measuring piezoelectric output-fact or friction?, Adv. Mater. 32 (2020), 2002979.
584 [44] H. Chen, L. Zhou, Z. Fang, S. Wang, T. Yang, L. Zhu, X. Hou, H. Wang, Z.L. Wang,
585 Piezoelectric nanogenerator based on in situ growth all-inorganic $CsPbBr_3$ perovskite
586 nanocrystals in PVDF fibers with long-term stability, Adv. Funct. Mater. 31 (2021),
587 2011073.
588 [45]R. Ding, X. Zhang, G. Chen, H. Wang, R. Kishor, J. Xiao, F. Gao, K. Zeng, X.
589 Chen, X. Sun, Y. Zheng, High-performance piezoelectric nanogenerators composed of
590 formamidinium lead halide perovskite nanoparticles and poly(vinylidene fluoride),
591 Nano Energy 37 (2017), 126-135.

[46] K. Maity, U. Pal, H.K. Mishra, P. Maji, P. Sadhukhan, Z. Mallick, S. Das, B. Mondal, D. Mandal, Piezo-phototronic effect in highly stable $CsPbI_3$-PVDF composite for self-powered nanogenerator and photodetector, Nano Energy 92 (2022), 106743.
[47] A. Sultana, M.M. Alam, P. Sadhukhan, U.K. Ghorai, S. Das, T.R. Middya, D. Mandal, Organo-lead halide perovskite regulated green light emitting poly(vinylidene fluoride) electrospun nanofiber mat and its potential utility for ambient mechanical energy harvesting application, Nano Energy 49 (2018), 380-392.
[48] R. Tusiime, F. Zabihi, M. Tebyetekerwa, Y.M. Yousry, Y. Wu, M. Eslamian, S. Yang, S. Ramakrishna, M. Yu, H. Zhang, High stress-driven voltages in net-like layer-supported organic–inorganic perovskites, J. Mater. Chem. C 8 (2020), 2643-2658.
[49] S. Si, S. Paria, S.K. Karan, S. Ojha, A.K. Das, A. Maitra, A. Bera, L. Halder, A. De, B.B. Khatua, In situ-grown organo-lead bromide perovskite-induced electroactive gamma-phase in aerogel PVDF films: an efficient photoactive material for piezoelectric energy harvesting and photodetector applications, Nanoscale 12 (2020), 7214-7230.
[50] G. Huang, A.A. Khan, M.M. Rana, C. Xu, S. Xu, R. Saritas, S. Zhang, E. Abdel-Rahmand, P. Turban, S. Ababou-Girard, C. Wang, D. Ban, Achieving ultrahigh piezoelectricity in organic–inorganic vacancy-ordered halide double perovskites for mechanical energy harvesting, ACS Energy Lett. 6 (2020), 16-23.

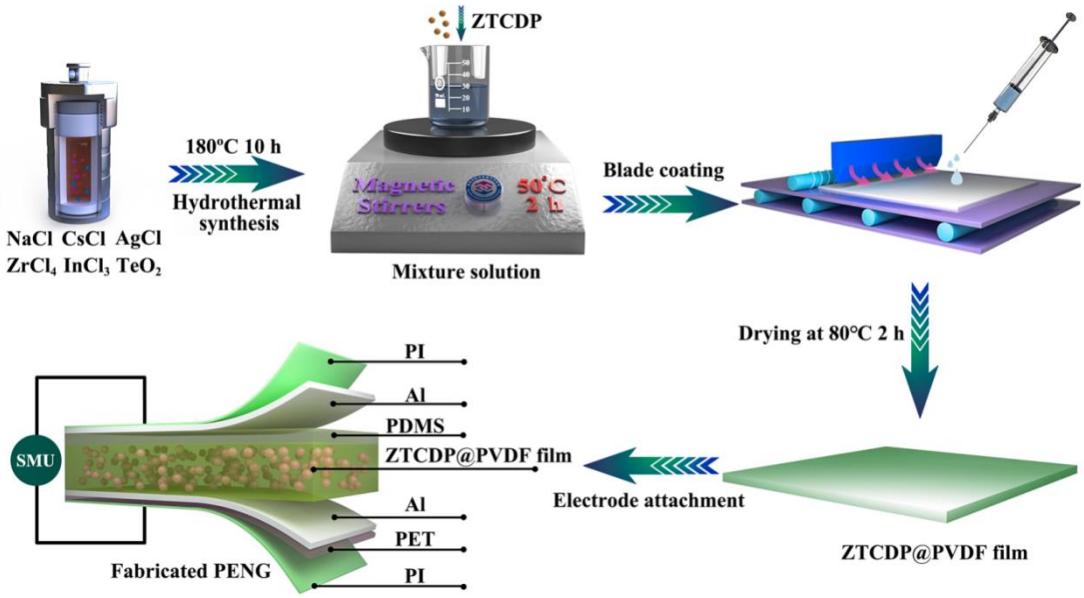

Fig. 1. Schematic illustration on the fabrication process for assembling a flexible PENG based on ZTCDP@PVDF.

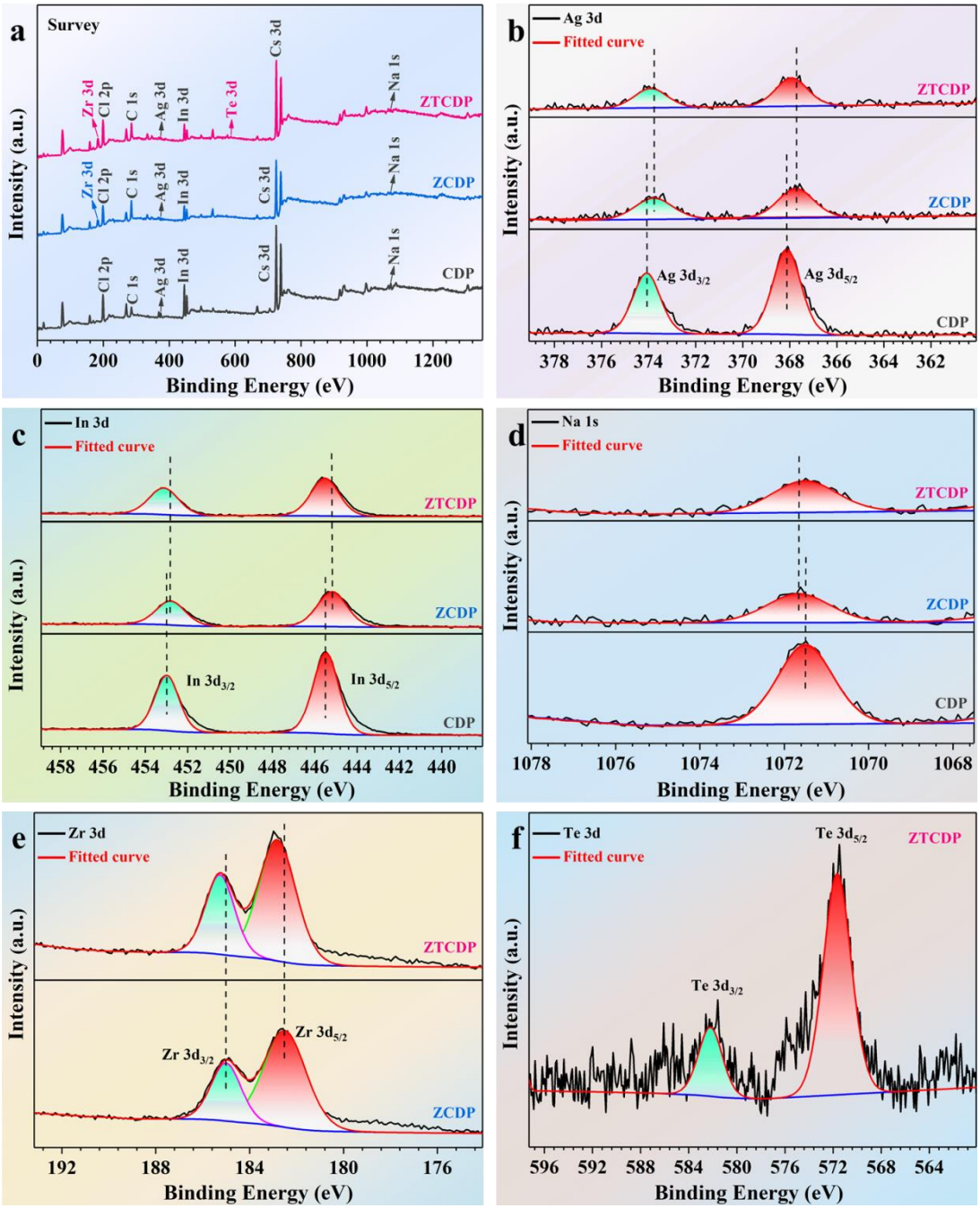

Fig. 2. XPS spectra of the CDP, ZCDP, and ZTCDP samples. a) Survey spectrum. b-f) High-resolution spectra of Ag 3*d*, In 3*d*, Na 1*s*, Zr 3*d* and Te 3*d*, respectively.

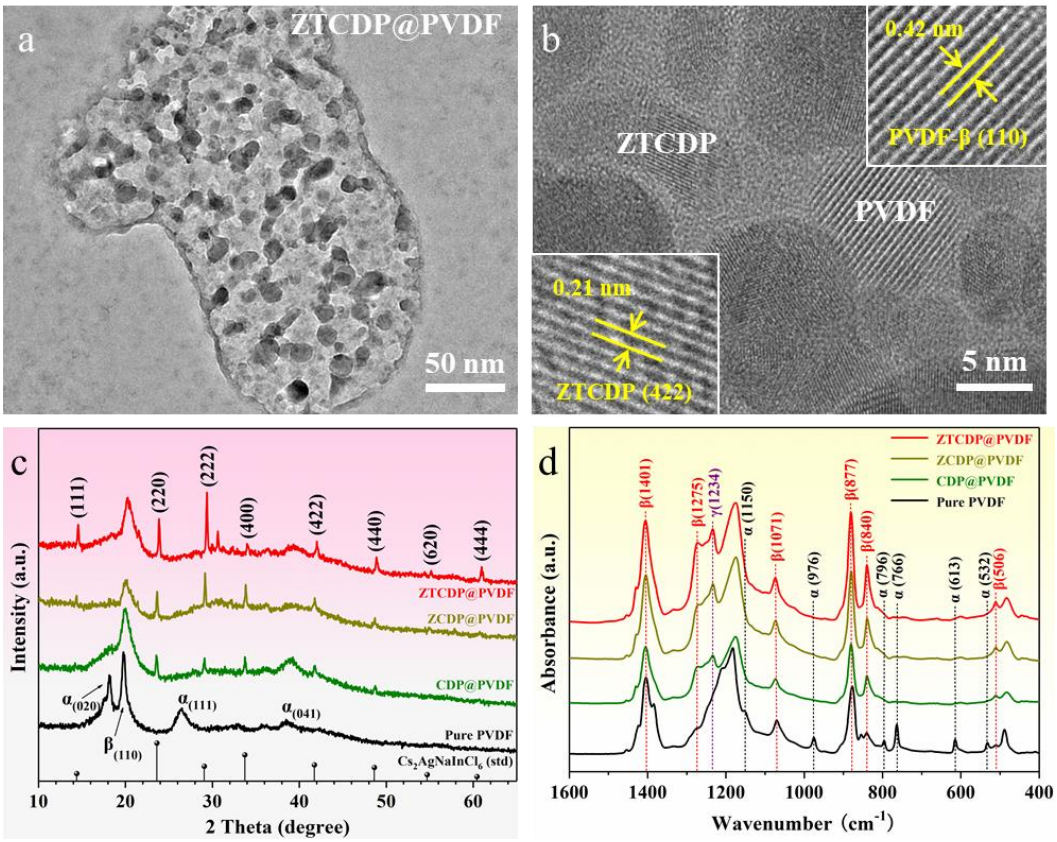

Fig. 3. a-b) Typical TEM and HRTEM images of ZTCDP@PVDF samples. c-d) Typical XRD patterns and FT-IR spectra of pure PVDF, CDP@PVDF, ZCDP@PVDF, and ZTCDP@PVDF samples.

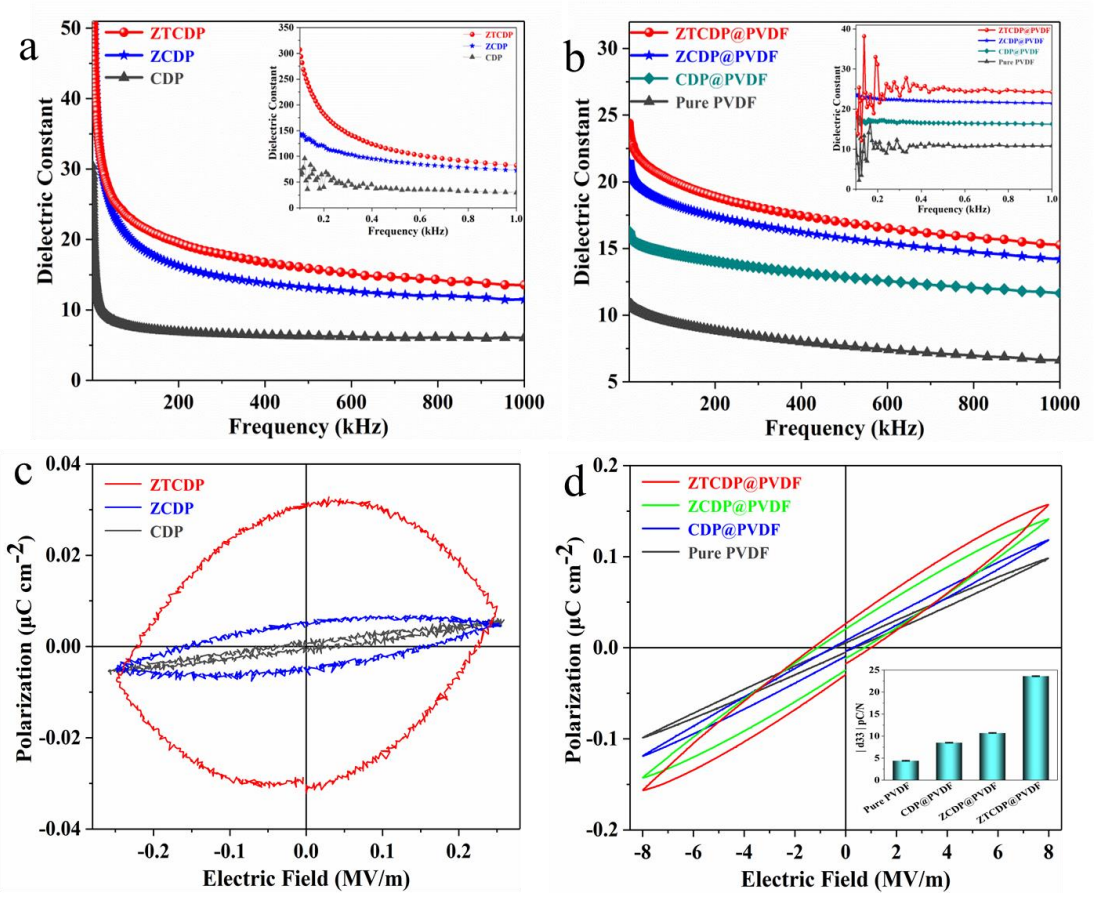

Fig. 4. a-b) Dielectric constants of a) CDP, ZCDP, and ZTCDP samples and b) pure PVDF, CDP@PVDF, ZCDP@PVDF, and ZTCDP@PVDF samples at different frequencies (1-1000 kHz), the insets of a) and b) show those at low frequency (0.1 - 1 kHz). c-d) Room-temperature P-E hysteresis loops of c) CDP, ZCDP, and ZTCDP samples and d) pure PVDF, CDP@PVDF, ZCDP@PVDF, and ZTCDP@PVDF samples. The inset is d_{33} piezoelectric coefficients of pure PVDF, CDP@PVDF, ZCDP@PVDF, and ZTCDP@PVDF samples.

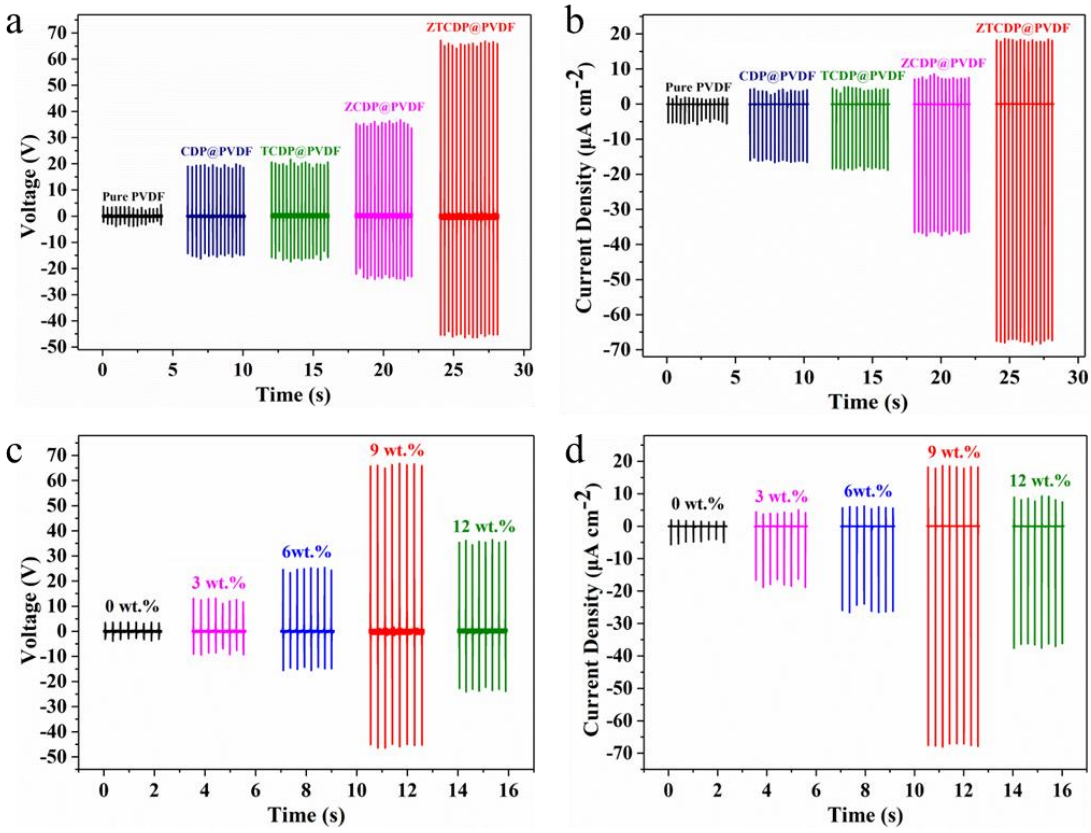

Fig. 5. a) Open circuit voltages (V_{oc}) and b) short circuit current densities (I_{sc}) of PENGs based on pure PVDF, CDP@PVDF, TCDP@PVDF, ZCDP@PVDF and ZTCDP@PVDF. c) V_{oc} and d) I_{sc} of PENGs based on ZTCDP@PVDF with different ZTCDP contents.

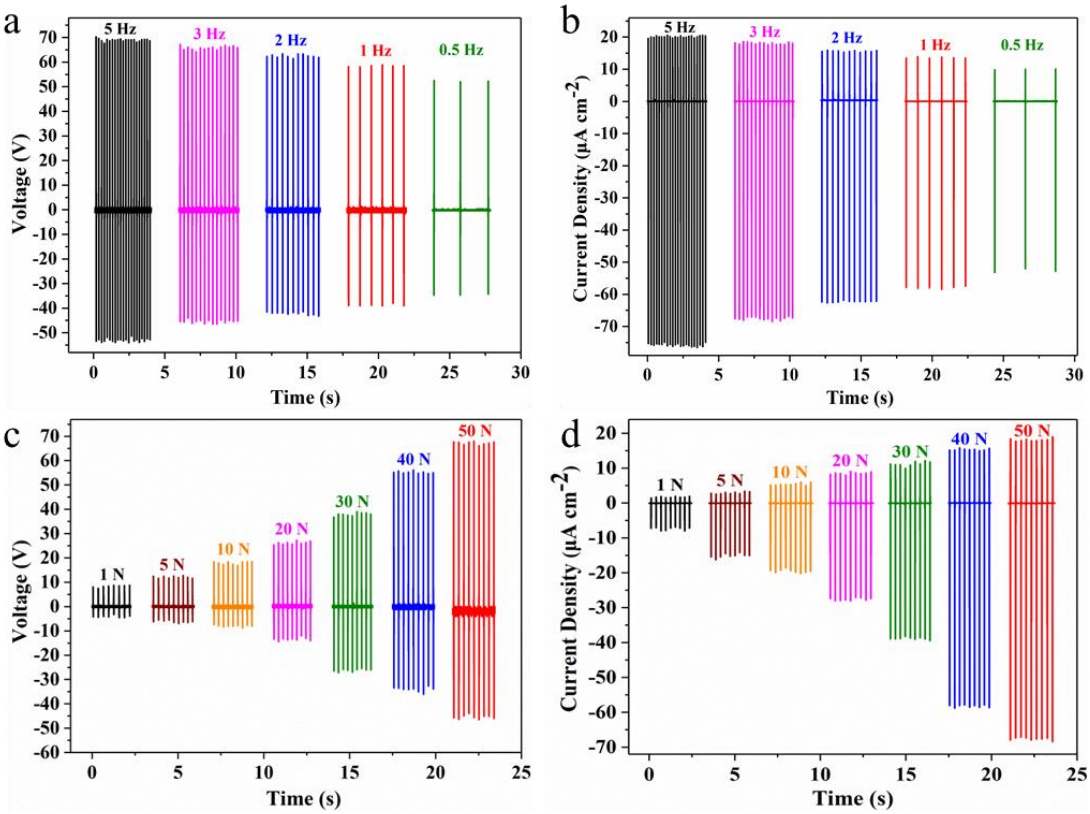

Fig. 6. a-b) V_{oc} and I_{sc} of the PENGs based on 9 wt.% ZTCDP@PVDF at different frequencies and c, d) V_{oc} and I_{sc} of the PENGs based on 9 wt.% ZTCDP@PVDF at different applied forces.

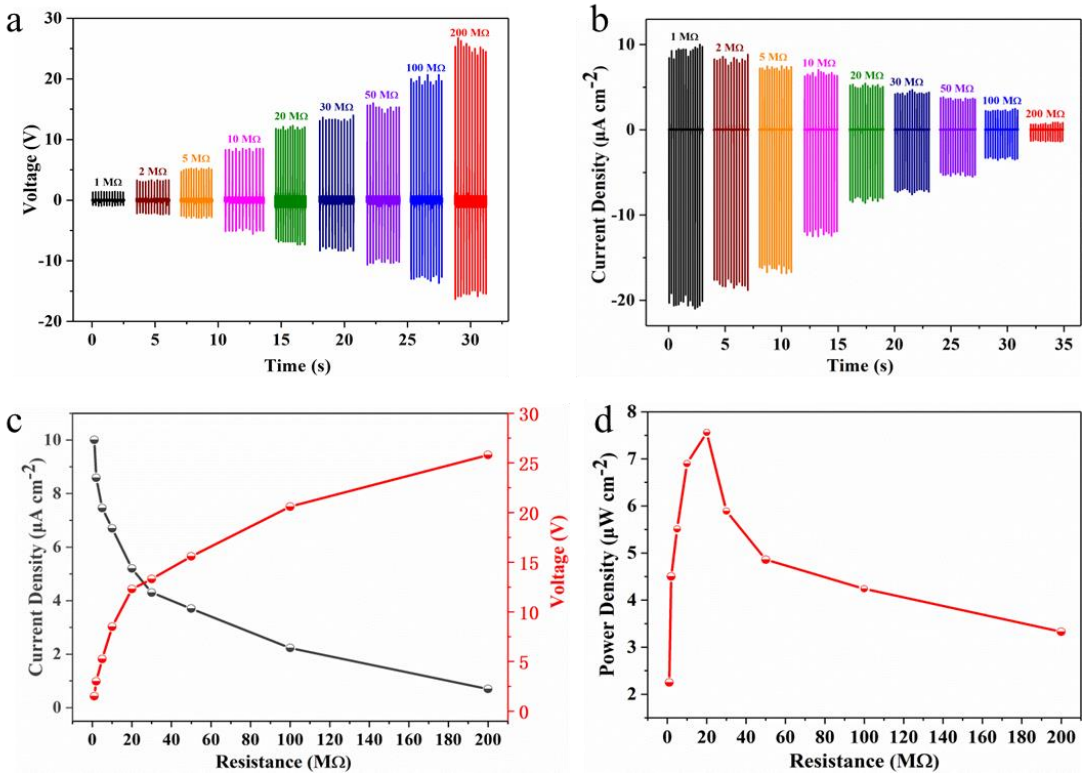

Fig. 7. a-b) V_{oc} and I_{sc} of the PENGs based on 9 wt.% ZTCDP@PVDF under different external load resistances from 1 to 200 MΩ. c-d) The variations of V_{oc}, I_{sc}, and power densities with loaded resistances.

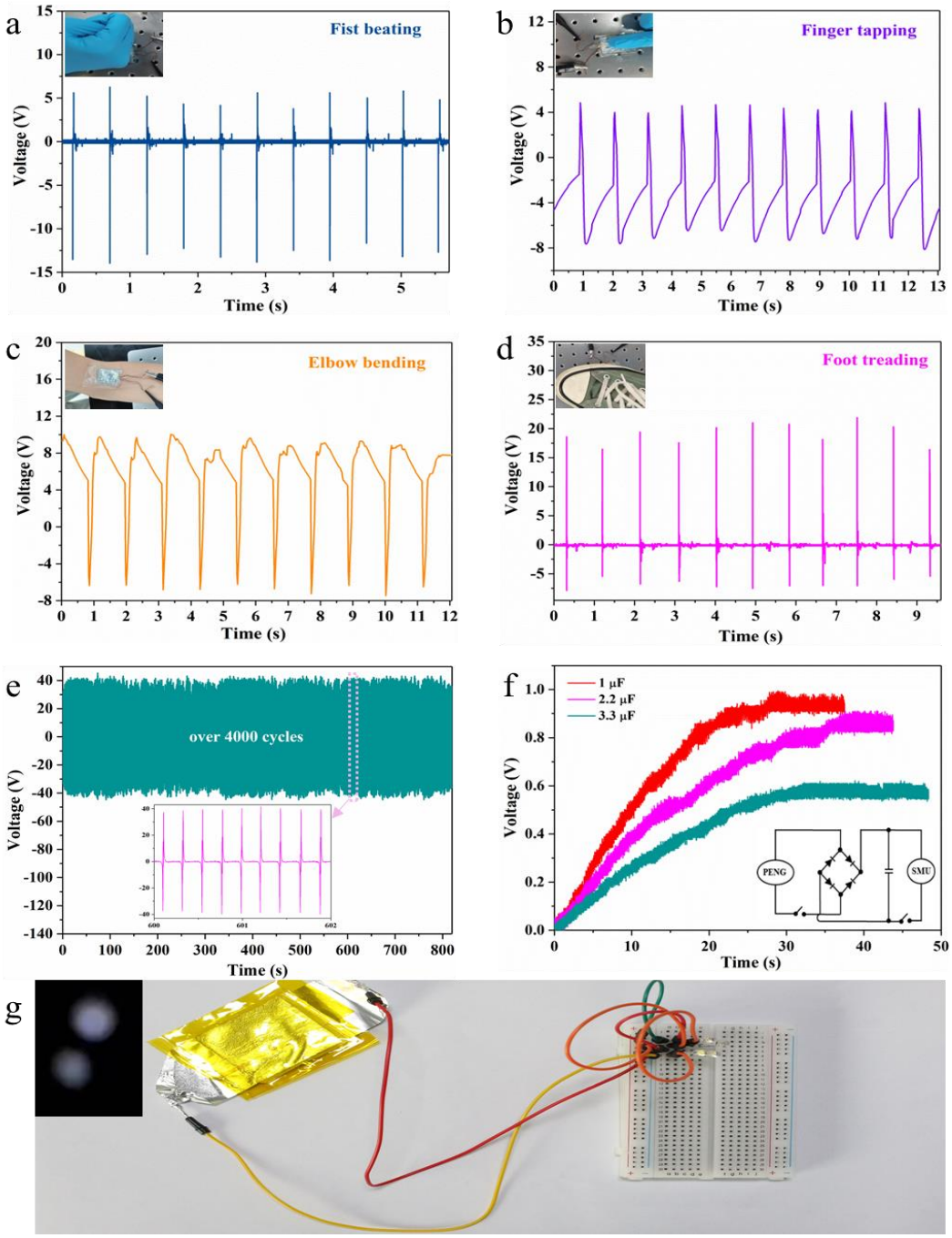

Fig. 8. a-d) V_{oc} of the PENGs based on 9 wt.% ZTCDP@PVDF subjected to different body movements of fist beating, finger tapping, elbow bending and foot treading, respectively. e) The stability of the PENGs based on 9 wt.% ZTCDP@PVDF over 4000 cycles. The inset gives the amplified view of V_{oc} from 600 to 602 s. f) Charging curves of the capacitors with different capacitance values by the PENGs based on 9 wt.% ZTCDP@PVDF after bridge rectification. The inset is the rectifier circuit diagram with the PENG. g) Optical image for lighting the LEDs. The inset shows two lighting LEDs.

Table 1. Overview on the piezoelectric output performances of typically reported PENGs.

Materials	Preparation method	V_{oc}	I_{sc}	Mode	Active area [cm^2]	Thickness [μm]	Ref.
$CsPbBr_3$-P(VDF-TrFE)	Casted	2.4 V	160 nA cm^{-2}	Pressing	1 × 1	-	[13]
$MAPbI_3$-PVDF	Casted	1.8 V	37.5 nA	Pressing	-	~20	[16]
PPy-P(VDF-HFP)	Casted	20.08 V	1 μA cm^{-2}	Pressing	1.5 × 2	~60	[9]
$FAPbBr_3$-PVDF	Casted	30 V	6.2 μA cm^{-2}	Pressing	1.2 × 1.4	125	[45]
$CsPbI_3$-PVDF	Casted	20 V	6 μA	Pressing	2 × 0.1	~160	[46]
$MAPbBr_3$-PVDF	Electrospinning	5 V	60 nA	Pressing	2.4 × 1.5	-	[47]
$CsPbBr_3$-PVDF	Electrospinning	103 V	170 μA cm^{-2}	Pressing	1.5 × 2	180	[44]
$CsPbBr_3$-PVDF	Electrospinning	33 V	300 nA cm^{-2}	Pressing	1 × 1	90	[22]
$MAPbI_3$-SnO_2-PVDF	Electrospinning	4.82 V	29.7 nA	Bending	0.25 × 0.25	-	[48]
$FAPbBr_3$-PVDF	In-situ growth	26.2 V	2.1 μA	Pressing	1.5 × 2	-	[49]
$TMCM_2SnCl_6$-PDMS	Casted	81 V	2 μA	Pressing	>5 × 5	400	[50]
Cs_2SnI_6-PVDF	In-situ growth	9 V	5 μA	Pressing	~2 × 2	-	[18]
Zr/Te codoped $Cs_2Ag_{0.3}Na_{0.7}InCl_6$@PVDF	**Casted**	**67 V**	**18 μA cm^{-2}**	**Pressing**	**1 × 1**	**~100**	**This work**

Xiangcong He received his Bachelor of polymer Materials and Engineering from Institute of new technology of hubei university of engineering in 2020. Now he is learning at the School of Materials Science and Chemical Engineering of Ningbo University for a master's degree. His current research mainly focuses on the research and applications of flexible electronic devices with functional polymer films.

Prof. Jinju Zheng received her Ph.D. degree in Condensed Matter Physics from University of Chinese Academy of Sciences. She is currently a professor at Ningbo University of Technology. Her main research focuses on the optical properties of semiconductor nanomaterials and their optoelectronic device applications.

Tao Yang received his Ph.D. in State Key Laboratory of Advanced Metallurgy from University of Science and Technology Beijing in 2018. Now he is a professor in Institute for Carbon Neutrality, University of Science and Technology Beijing. His current research mainly focuses on the application of electrochemistry in the field of energy.

Deliu Ou is currently pursuing his Master degree in the School of Guangxi University. His current research mainly focuses on the research and applications of solar cell with perovskite semiconductor material.

Chris R. Bowen has a BSc degree in Materials Science from the University of Bath (1986-1990) and a DPhil in Ceramics from the University of Oxford (1990-1993). Post-doctoral work has been undertaken at Tecnische Universität Harburg-Hamburg and University of Leeds (1994-1996). He was Senior Scientist at the Defence Evaluation and Research Agency from 1996-1998 and joined the University of Bath as a Lecturer in 1998 and is now Professor of Materials. He was a former ERC Advanced Investigtor (2013-2018) and is currently a UKRI Frontier Research Guarantee Holder on Processing of Smart Porous Electroceramic Transducers (ProSPECT), 2023-2028; Project No. EP/X023265/1.

Songhan Shi is currently pursuing his Master degree in the School of Materials Science and Chemical Engineering, Ningbo University. His research interests include ferroelectric ceramics, nanocomposites and their applications in energy storage, conversion and management.

Qiaochu Chen received his Ph.D. from Hunan University of Technology. His current research mainly focuses on the research and applications of optical devices with perovskite semiconductor materials.

Dr. Hui Fu received her Ph.D. degree in Materials Science and Engineering from Guizhou University. She works in Ningbo University of Technology (NBUT), and is a member of Institute of Micro/Nano Materials and Devices in NBUT. Dr. Fu has published more than 10 peer-reviewed papers in the field of semiconductor nanocrystals and their applications.

Prof. Mark Huang received his Ph.D. degree in Polymer Chemistry from The Institute of Chemistry, Chinese Academy of Science and was a Postdoctoral Fellow at National University of Singapore. He is currently Anzhong Chair Professor at Ningbo University and Distinguished Professor at Shenzhen University. Dr. Mark Huang was a Senior Process Engineer at Hitachi Chemical Asia/Pacific, a Principal Engineer at Micron Semiconductor Asia, Director of Unisteel Technology Group Company in Singapore. Dr. Huang severed Speed Wireless Technology as CTO being in charge of TSV fabrication, CIS WLP and finger print sensor (FPS) packaging.

Prof. Yumin Ye received his Ph.D. in Biosystems Engineering from Oklahoma State University, USA. After that, he did post-doc research in the Department of Materials Science and Engineering in University of Wisconsin-Madison, USA. He is currently an associate professor in Ningbo University, China. His main research interests lie in vapor-based synthesis of functional polymer and their applications in electronic devices, biomedical engineering, and surface modifications. Details can be found at: www.yeyumingroup.cn

Xiaocheng Huang received his Bachelor of Metallurgical Engineering from Wuhan University of Science and Technology in 2020. Now he is pursuing Master degree in the School of Materials Science and Chemical Engineering at Ningbo University. His main research direction is chemical vapor deposition of superwettable polymer coatings and biomimetic polymer nanostructures.

Dr. Wenna Liu received her Ph.D. from University of Science and Technology Beijing. She is currently a lecturer at Ningbo University. Her main research interests lie in conductive polymer and their application in energy storage.

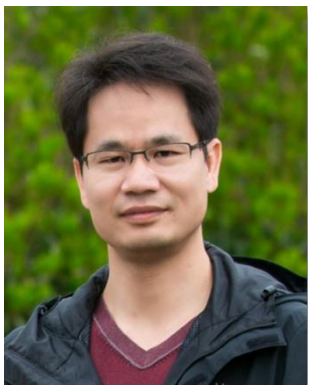

Prof. Dr. Weiyou Yang received his Ph.D. degree in Materials Science and Engineering from Tsinghua University. He works in Ningbo University of Technology (NBUT), and is currently the leader of Institute of Micro/Nano Materials and Devices in NBUT. Dr. Yang has published more than 200 peer-reviewed papers in the field of low-dimensional inorganic nanomaterials and their applications. He has been elected as the Academician (foreign member) from Academy of Technological Sciences of Ukraine, and Fellow of Royal Society of Chemistry (FRSC), and awarded as a prominent expert for enjoying State Council Special Allowance of China.